ORIGINAL ARTICLE

East Asian summer monsoon response to anthropogenic aerosols redistribution: contrasting 1950–1980 and 1980–2010 to understand the role of non-Asian forcing

Zhinan Shao[1] · Hai Wang[1] · Yu-Fan Geng[1] · Chenrui Diao[2,3] · Yangyang Xu[3] · Xiao-Tong Zheng[1]

Abstract

Anthropogenic aerosols (AA) induce pronounced East Asian summer monsoon (EASM) changes since the industrial revolution. However, the regional contribution from different AA emission sources is hard to quantify due to AA's heterogeneous spatial distribution and the nonmonotonic trend at decadal time scale. Using coupled climate models from Coupled Model Intercomparison Project Phase 6 (CMIP6) and Community Earth System Model 1 (CESM1) large ensemble simulations, we investigate EASM responses between 1950–1980 and 1980–2010, to understand how the remote influence of changes in the AA emissions from Europe modulates the EASM at decadal time scale. AA emissions from Europe increased early in the latter half of the twentieth century and then decreased rapidly after the 1980s. During 1950–1980, the increase of AA emissions from Europe, together with the localized increase of AA emissions from East Asia, weakens the EASM by generating the tropospheric cooling and shifting the East Asian subtropical jet equatorward. However, during 1980–2010, the declined AA emissions from Europe generate the tropospheric warming and induce an atmospheric teleconnection pattern that initiate at the heating anomaly and propagate downstream to northeast Asia following the westerly jet, leading to an enhanced EASM. This enhancement due to the remote influence of declined AA emissions from Europe explains why after the 1980s, despite the localized increase of AA emissions from East Asia, coupled climate models results show that the EASM is intensified by the anomalous southerlies and the precipitation increase in Northeast Asia. Our results imply that at the long-term change view, the local AA emissions dominate the EASM response, while the non-local European AA emissions play a more important role in shaping the decadal EASM changes.

✉ Hai Wang
   wanghai@ouc.edu.cn

1   Key Laboratory of Physical Oceanography and Frontiers Science Center for Deep Ocean Multispheres and Earth System, College of Oceanic and Atmospheric Sciences, Ocean University of China, Qingdao 266100, Shandong, China

2   Department of Atmospheric Science, Colorado State University, Fort Collins, CO 80521, USA

3   Department of Atmospheric Sciences, Texas A&M University, College Station, TX 77843, USA

1 Introduction

The East Asian summer monsoon (EASM) provides about 60–70% of the annual mean precipitation in northern China (Ding and Chan 2005; Lei et al. 2011), which brings tremendous impacts on water resources, agricultures, economies, and ecosystems (Ma et al. 2017). Observations have revealed a robust decadal variation of the EASM, which leads to the shift of the precipitation and the associated risk of flood/drought over East Asia (Zhou et al. 2009), featuring the "southern flood and northern drought" precipitation pattern in China since the 1980s (Gong and Ho 2002; Zhou et al. 2009; Li et al. 2015, 2018; Zhang and Zhou 2015). Understanding the dynamical mechanism of the decadal EASM changes in a changing climate has important societal implications.

The EASM is an interactive system influenced by both internal variability at various time scales and external forcings due to either greenhouse gases (GHG) or anthropogenic aerosols (AA) emissions (Lei et al. 2011; Song et al. 2014). The dynamics of the decadal variation of the EASM have drawn much attention in recent years. Some studies have attributed it to internal climate variability, such as the phase transition of the Pacific Decadal Oscillation in the late 1970s (Yoon and Yeh 2010; Feng et al. 2014), and the changes of western Pacific subtropical high (Zhang et al. 2004; Choi and Kim 2019; Xu et al. 2020). However, since the industrial revolution, there was a dramatic increases in both GHG and AA emissions, having caused pronounced regional climate changes (Myhre et al. 2013; Bellouin et al. 2020). Thus, one cannot solely use the internal climate variability or the external forcing to explain the observed decadal EASM changes. We believe that it is important to evaluate the relative contribution of internal climate variability and external forcing to the observed EASM changes. While in this work, we put our focus on the externally forced decadal EASM variations.

Previous studies indicated that GHG forcing influences the EASM in complicated ways. The GHG-driven increase in atmospheric moisture may promote the wet EASM region following the "rich-get-richer" mechanism (Trenberth 2011). In addition, under the GHG forcing, the atmospheric circulation change may also lead to an increase in moisture convergence from ocean to land (Kitoh et al. 2013; Lee and Wang 2014), which further enhance the atmospheric moisture and surface evaporation, resulting in the strengthened EASM. Moreover, the GHG-induced oceanic slow response may weaken both the Hadley and Walker cells, which lead to the equatorward shift of the EASM rain-band (Zhou et al. 2019). Although the GHG forcing has caused warming and enhanced EASM trends, it can hardly explain the decadal EASM variations as the GHG emissions increased steadily since the industrial revolution. Besides, mounting evidences pointed to the importance of AA emissions in weakening the EASM (Bollasina et al. 2011; Wu et al. 2013; Liu et al. 2017; Wang et al. 2019). The weakening effect of the AA forcing has probably masked the otherwise positive response of monsoon rainfall due to GHG forcing (Singh 2016), fueling a large body of research on the complicated dynamics of the AA induced EASM changes (Li et al. 2016).

The AAs' effect on EASM can be decomposed into a direct atmospheric response to radiative forcing without sea surface temperature (SST) changes (Li et al. 2018), and a SST-mediated coupled ocean–atmosphere interaction response (Ganguly et al. 2012; Wang et al. 2019). For the AA induced direct atmospheric response, the scattering aerosols (such as sulfate aerosols) play a "dimming" effect primarily over land, which act to weaken the land-sea thermal contrast over the Asian continent and the adjacent western Pacific, leading to the weakening of the EASM (Li

et al. 2016; Wang et al. 2017; Mu and Wang 2021). However, the absorbing aerosols (such as black carbon) play a "heating" effect by absorbing the solar radiation, and act to strengthen the EASM (Li et al. 2016; Wang et al. 2017; Mu and Wang 2021). Furthermore, the carbonaceous-aerosol-induced Tibetan Plateau snowpack pollution can also influence the East Asian hydrological cycle and monsoon system (Qian et al. 2011).

In synergy with the direct atmospheric response, the AA induced SST change also plays an important role in shaping the long-term EASM response. AA mainly emitted and concentrated in the Northern Hemisphere can generate an inter-hemisphere asymmetric SST pattern and atmospheric circulation anomalies in the tropics (Wang et al. 2016a, b) governed by the cross-equatorial energy transport theory (Kang et al. 2008), which further brings anomalous descent in the Northern Hemisphere subtropics, and leads to the weakening of EASM (Wang et al. 2019). In addition to the hemispheric influences, the regional AA emission in Asia may also lead to a local SST cooling in the Northwest Pacific which further induce an anomalous meridional atmospheric overturning circulation, resulting in the weakening of EASM (Song et al. 2014; Wang et al. 2019; Li et al. 2020; Wang et al. 2021b).

The early studies provided a general understanding that the localized AA emissions in East Asia can weaken the EASM, albeit with complicated physical mechanism. However, recent studies implied that the European aerosol emissions reductions may induce stronger global and regional precipitation increases beyond the emissions source regions (Westervelt et al. 2018), especially when normalized by unit radiative forcing or by aerosol burden change (Liu et al. 2018). Therefore, besides the localized AA forcing, remote influence of non-local AA emissions has been proved to play an important role in modulating the EASM response (Dong et al. 2016; Wang et al. 2017). Climate model results indicate that the AA emission from Europe can not only influence the local climate response in Europe, but also modulate the EASM by changing the upper tropospheric thermal structure in the Northern Hemisphere mid-latitudes (Wang et al. 2017, 2020). The anomalous cooling/heating of the Eurasian troposphere due to the increasing/decreasing emissions of AA from Europe can further influence both the position and intensity of the mid-latitude westerly jet through thermal wind balance, and result in the EASM anomaly (Lin et al. 2018; Undorf et al. 2018; Mu and Wang 2021; Dong et al. 2022).

Most of the studies explored the EASM response to local and non-local AA forcing using long-term trends during which the regional AA emissions show monotonic increase over East Asia or Europe, or contrasting two different states between the pre-industrial and the conditions in around 2000s. However, unlike the well-mixed GHGs, the spatial

distribution of AA emissions changes rapidly since the industrial revolution. Understanding the evolving contribution of AA forcing to the climate response is of great importance to climate change detection and attribution. Wang et al. (2015) revealed the climatic impacts of the west-to-east shift in AA emissions focusing on the fast response of the atmospheric system over the globe. Recently, the evolving patterns of large-scale coupled ocean–atmosphere responses to AA and GHG forcing were evaluated with different fully coupled climate models (Deser et al. 2020; Diao et al. 2021; Wang and Wen 2022). In addition to these large-scale climate responses to the spatial and temporal variations of AA forcing, how the EASM will respond to the spatial redistribution of AA forcing at decadal time scale remains to be investigated.

Inspired by these existing progresses, here we quantify the EASM response to the spatial and temporal changes in AA since the mid-twentieth century based on the latest Coupled Model Intercomparison Project Phase 6 (CMIP6) historical AA single-forcing and all-forcing simulations. By comparing the EASM response patterns in different historical periods featuring distinct AA forcing patterns, we highlight the relative importance of local (Asian) and remote (non-Asian) AA forcing in shaping the decadal EASM anomalies. Furthermore, we reveal the dynamical mechanism of how the non-local AA forcing from Europe regulates the EASM response using a set of idealized regionally forced single-forcing experiments based on a fully coupled large-ensemble simulation. This study aims to expands our understanding of AA influence on EASM from a simplistic perspective of long-term overall change to a more detailed perspective that includes the spatial and temporal evolutions at finer scales, which has important implications for regional climate change attribution and projection.

The rest of the paper is organized as follows. Section 2 provides description of the multi-model simulations, idealized model experiments, and analytical methods. Section 3 describes the evolution of AA emissions and identifies the leading modes of regional climate response due to the evolving AA forcing. Section 4 reveals how the distinct patterns of AA forcing in the two different historical periods shaped the decadal EASM responses. Section 5 specifically evaluates the role of AA emissions changes from Europe in regulating the EASM responses after the 1980s. Section 6 provides a summary with further discussion.

2 Data and methods

To isolate the time-varying role of variations of AA forcing in shaping the EASM response, we use twelve historical AA single-forcing (Hist-Aer) simulations and historical all-forcing simulations which include both anthropogenic and natural forcings from the Detection and Attribution Model Intercomparison Project (DAMIP) in the CMIP6 dataset (Table 1, Erying et al. 2016; Pascoe et al. 2019). In the Hist-Aer simulations, AA are the only time-evolving forcing agent with the other forcings fixed at the preindustrial level. The AA emission changes are represented by the 550 nm aerosol optical depth (AOD) changes with nine of the twelve models output this variable. To further identify the influence of distinct AA forcing patterns on the observed EASM changes, we use the fifth generation European Centre for Medium-Range Weather Forecasts atmospheric reanalysis (ERA5) (Hersbach et al. 2020) to examine the 850 hPa wind changes and precipitation anomalies during 1950–2010.

To eliminate the internal variability and the inter-model uncertainty, we first obtain the multi-member ensemble for each model (ensemble size shown in Table 1) and then construct the multi-model ensemble mean results. The internal climate variability is indeed important in interpreting the climate response to AA forcing for small ensembles (Oudar et al. 2018; Diao et al. 2021). The role of internal climate variability can be better estimated with the use of large ensemble approach (Deser et al. 2020). In this study, we omit the internal climate variability and focus on the externally forced regional climate change. To facilitate inter-model comparison, all the model outputs are interpolated onto a common grid of 144 (zonal) × 73 (meridional) grid points (2.5° horizontal resolution) with 12 vertical layers from 1000 to 100 hPa.

In addition to the CMIP6 Hist-Aer simulations, we also use large ensembles based on the Community Earth System Model 1 (CESM1): (1) the all-forcing simulations (CESM1-LENS, Kay et al. 2015); (2) the single-forcing simulations (Fix_FF1920, Deser et al. 2020); (3) the "Western Hemisphere" (WH) experiments (Fix_WestFF1920, Diao et al. 2021). The CESM1-LENS simulations include a 40-member ensemble of fully coupled simulations for the period of 1920–2100 with historical radiative forcing during 1920–2005 and RCP8.5 scenario thereafter. The Fix_FF1920 simulations include a 20-member ensemble of simulations with the industrial aerosols fixed at 1920. It should be emphasized that in the timing (the year 1920) of the leveling emission here, AA emissions are not removed entirely but rather stay at a relatively low level. The WH experiments, help to gain further insights on the role of WH AA forcing, include a 10-member ensemble branched from the existing run of Fix_FF1920 simulations. In this experiment, the same initialization protocol as Fix_FF1920 were used by only the AA emissions over the WH (20°N–80°N, 130°W–10°W and 30°N–80°N, 10°W–40°E) were fixed, with AA emissions over other regions were allowed to evolve during 1980–2020 (Diao et al. 2021). This experiment was conducted from 1920 through 1980 for one realization and then was expanded to 10 ensemble members for

Table 1 The CMIP6 historical all-forcing and Hist-Aer simulations used in this study

Model name	Institution	Ensemble size	
		aerosol optical depth at 550 nm (od550aer)	Other variables
ACCESS-CM2	Commonwealth Scientific and Industrial Research Organisation, Australia; Australian Research Council Centre of Excellence for Climate System Science	3	3
ACCESS-ESM1-5	Commonwealth Scientific and Industrial Research Organisation, Australia	3	3
BCC-CSM2-MR	Beijing Climate Center, China	–	3
CNRM-CM6-1	Centre National de Recherches Meteorologiques, France; Centre Europeen de Recherche et de Formation Avancee en Calcul Scientifique, France	3	10
CanESM5	Canadian Centre for Climate Modelling and Analysis, Canada	15	15
FGOALS-g3	Chinese Academy of Sciences, China	–	3
GFDL-ESM4	National Oceanic and Atmospheric Administration, Geophysical Fluid Dynamics Laboratory, USA	–	1
HadGEM3-GC31-LL	Met Office Hadley Centre, UK	4	4
IPSL-CM6A-LR	Institut Pierre Simon Laplace, France	10	10
MIROC6	Japan Agency for Marine-Earth Science and Technology, Japan; Atmosphere and Ocean Research Institute, The University of Tokyo, Japan; National Institute for Environmental Studies, Japan; RIKEN Center for Computational Science, Japan	10	10
MRI-ESM2-0	Meteorological Research Institute, Japan	5	5
NorESM2-LM	NorESM Climate modeling Consortium consisting of Center for International Climate and Environmental Research, MET-Norway, Nansen Environmental and Remote Sensing Center, Norwegian Institute for Air Research, University of Bergen, University of Oslo, and Uni Research, Norway	3	3

1980–2020. The difference between the CESM1-LENS and the WH experiments therefore can be used to quantify the climate response due to AA emissions changes from the WH during 1980–2020. For the detailed experiments design, please refer to Diao et al. (2021).

Focusing on the EASM response to the evolving AA emissions, we calculate the boreal summer (June-July–August, JJA) seasonal mean 550nm AOD, precipitation, net radiative flux at top of the atmosphere (TOA, F_t) as defined in Eq. (1), atmospheric temperature, and circulation (including the sea level pressure (SLP), zonal (U) and meridional (V) wind.

$$\Delta F_t = \Delta(U_{tl} + U_{ts} - D_{ts}) \tag{1}$$

In Eq. (1), the F_t is evaluated to investigate the radiative effect of AA. U_{tl}, U_{ts}, D_{ts} indicate the upward longwave radiation, upward shortwave radiation, and downward shortwave radiation at the TOA, respectively.

We firstly perform an empirical orthogonal function (EOF) analysis on the precipitation change over the Eurasia region (0°–80°N, 0°–180°E) in the multi-model ensemble of CMIP6 Hist-Aer simulations during 1950–2010. Before the EOF analysis, a 9-year running average is applied to eliminate any residual high frequency variability. The EASM response to the spatial and temporal variation of AA forcing can be captured by the leading principal components (PCs)

of the EOF analysis. We then regressed the lower tropospheric (850 hPa) wind anomalies to the leading PCs of the EOF analysis in order to get the corresponding EASM circulation changes. We also regressed the 550 nm AOD changes to the leading PCs of the EOF analysis to evaluate the relative impact of local and non-local AA emissions changes to the EASM responses. In addition, we regress the 9-year low-pass filtered precipitation and 850 hPa wind anomalies onto the East Asian and European regional mean AOD changes during 1950–2010 in both climate model simulations and observations. Comparisons of these regressions highlight the role of the individual contributions of local and remote AA forcing to the observed EASM changes. Furthermore, to better describe the distinct contributions from different AA emissions patterns to the EASM changes, we calculate the linear trends in the multi-model ensemble of CMIP6 Hist-Aer and historical all-forcing simulations in three different periods (1950–1980, 1980–2010, and 1950–2010) based on the spatial and temporal evolutions of AA emissions. The statistical significance of the trend analysis is assessed at the 95% confidence level using Student's t test.

Finally, to highlight the role of Europe AA emissions changes in regulating the EASM responses, we calculated the point correlation between the European regional average (40°N–60°N, 10°E–50°E) and tropospheric average (850–200 hPa mean) temperature anomaly and the 200 hPa geopotential height anomaly in the North

Hemisphere (a 9-year running average is applied to eliminate any residual high frequency variability). The point correlation analysis revealed an atmospheric teleconnection response. To further describe this atmospheric teleconnection, we also used the wave-activity flux (Takaya and Nakamura 2001) to diagnose the propagation of wave packets of migratory and stationary eddies on a zonally varying basic flow as defined in Eq. (2):

$$W = \frac{P}{2|U|} \begin{pmatrix} U\left(\psi_x'^2 - \psi'\psi_{xx}'\right) + V\left(\psi_x'\psi_y' - \psi'\psi_{xy}'\right) \\ U\left(\psi_x'\psi_y' - \psi'\psi_{xy}'\right) + V\left(\psi_y'^2 - \psi'\psi_{yy}'\right) \end{pmatrix}, \quad (2)$$

where U and V represent the seasonal mean zonal and meridional wind, respectively. P is the pressure normalized at 1000hPa. $\psi\prime$ denotes the seasonal anomalous streamfunction at the 200hPa level, with the subscripts x and y referring to their partial differentials in the zonal and meridional direction, respectively.

3 AA induced EASM response: two modes distinct in space and time

The 550nm AOD change since the mid-twentieth century shows large spatial and temporal variations (Fig. 1), which may bring distinct regional climate responses. In East Asia, previous studies showed that not only the local AA emissions can regulate the EASM response by direct atmospheric response and SST mediated response (Wang et al. 2019), but also the European AA emissions may influence the EASM change by mediating the atmospheric temperature and circulation anomalies (Dong et al. 2016; Wang et al. 2017). For the East Asian AA emissions change, it shows monotonic increase during 1950–2010 and declines rapidly since 2013 (Fig. 1a) when China's Action Plan on the Prevention and Control of Air Pollution went into effect (Zheng et al. 2018; Samset et al. 2019; Wang et al. 2021a). In contrast, the AA emissions change in Europe shows a reversal trend during 1950–2010, which increases steadily during 1950–1980 and then decreases rapidly during 1980–2010 due to clean air regulations in the WH (Fig. 1b, c).
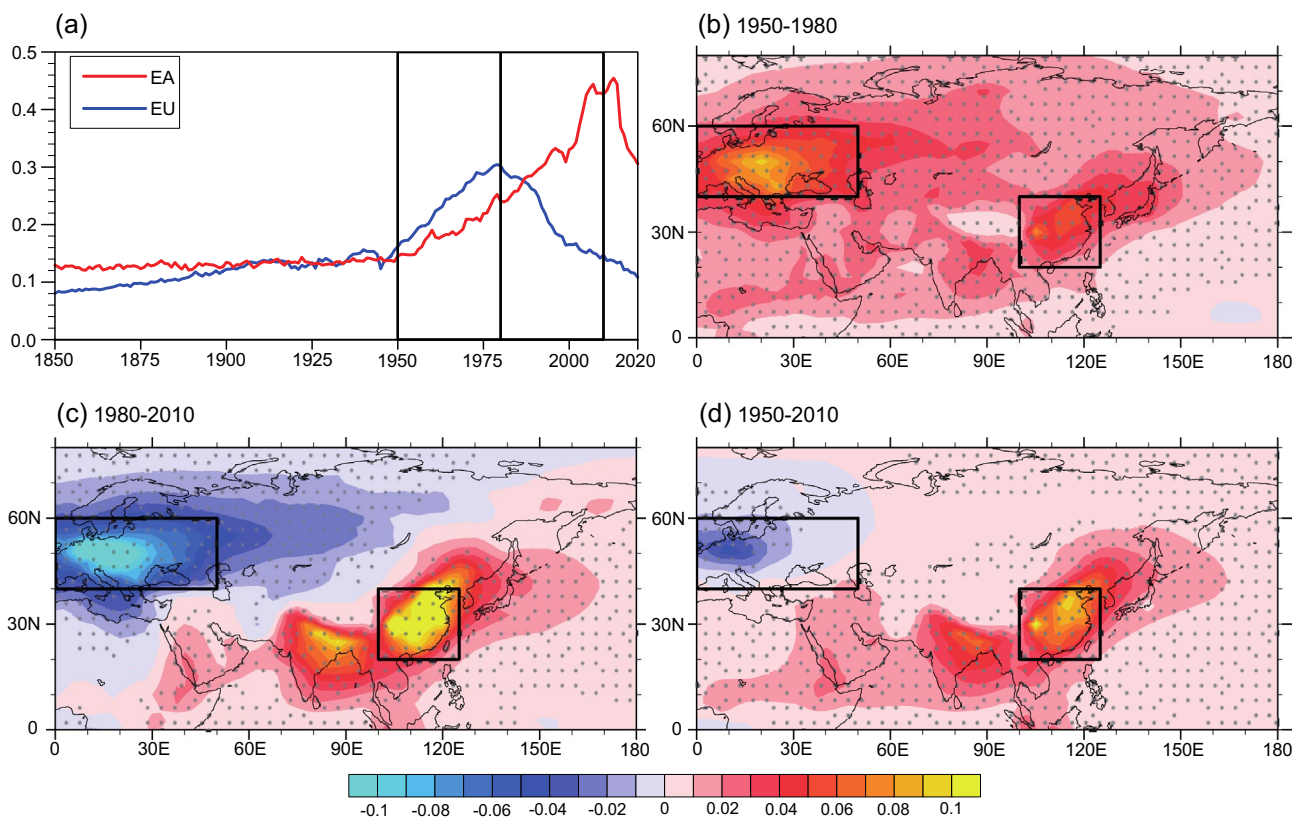

Fig. 1 **a** East Asian (red line, 100°E–125°E; 20°N–40°N) and European (blue line, 0°E–50°E; 40°N–60°N) regional mean Aerosol Optical Depth (ambient aerosol optical thickness at 550nm; unitless) changes from 1850 to 2020. Aerosol optical depth trend (unit: 1/decade) from **b** 1950–1980, **c** 1980–2010, **d** 1950–2010. Stippled regions indicate changes exceed 95% statistical confidence. All values are CMIP6 multi-model ensemble mean and boreal summer (JJA) seasonal mean

To reveal how the EASM may respond to the above two distinct AA emissions patterns since the mid-twentieth century, we firstly apply an EOF analysis on the low-frequency regional precipitation change during 1950–2010 in the Hist-Aer simulations (see Sect. 2 for details). Figure 2a and e show the leading spatial pattern and the corresponding PC time series, which explains about 53.8% of the total variance. The PC1 shows robust monotonic increase during 1950–2010 (Fig. 2e), which can be largely explained by the increase of AA emissions from East Asia (Fig. 2c). The spatial pattern of the precipitation anomaly shows a prominent decrease overall the EASM region with negative centers in South China, Indo-China Peninsula and northeast Bay of

Bengal (Fig. 2a). Corresponding to the decreased precipitation, the weakened monsoon circulation can be captured by the regression field of lower tropospheric (850hPa) winds with northeasterly anomalies south of 25°N. The drying trend and weakened EASM circulation can be attributed to both the atmospheric circulation responses generated by localized emissions of AA, and the large-scale meridional overturning circulation change in response to the inter-hemisphere asymmetric SST response (Wang et al. 2019; Li et al. 2020).

The first EOF mode reveals the EASM response to the monotonic increase of AA emissions from East Asia. However, this mode cannot completely represent the EASM
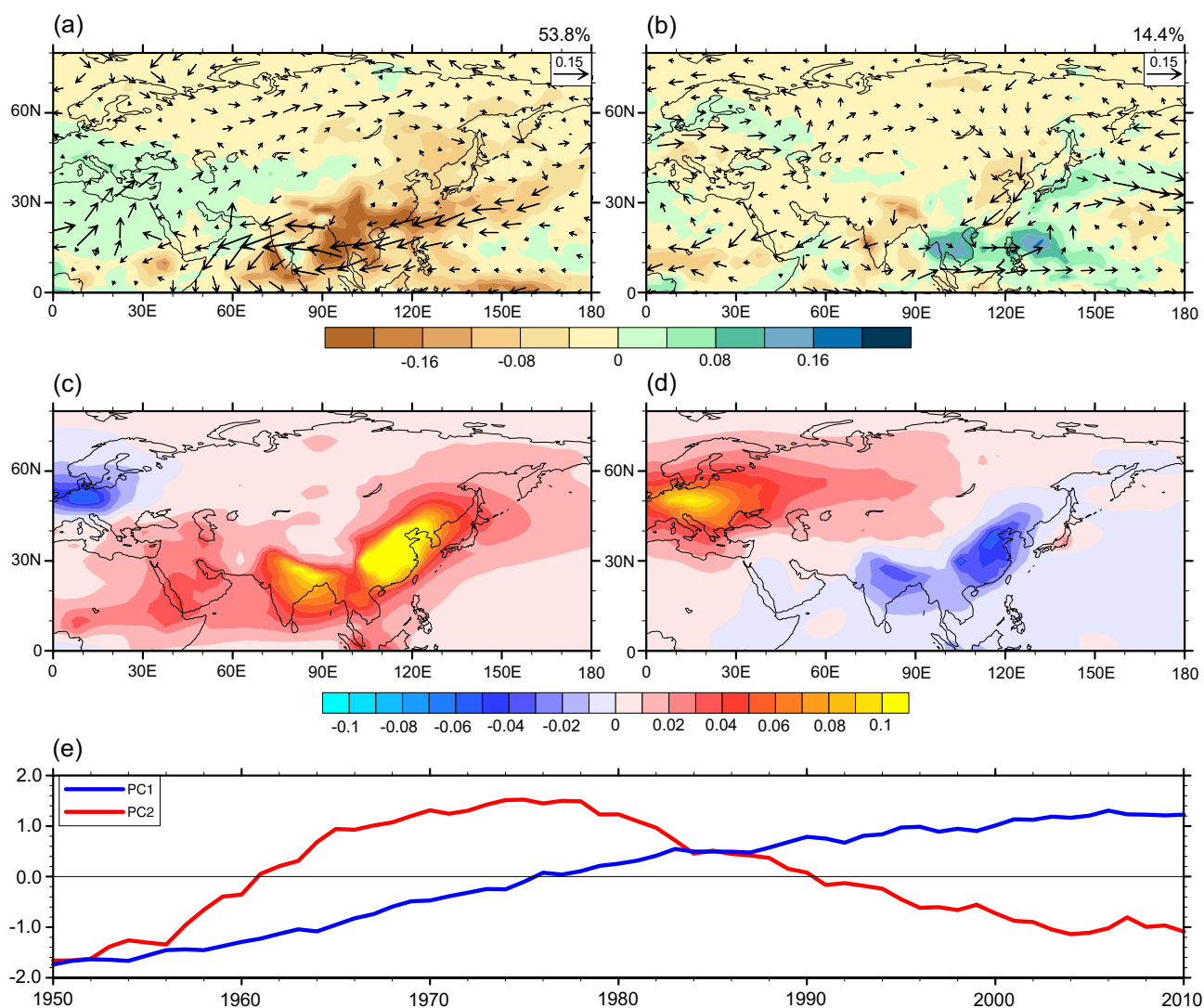
Fig. 2 The first (**a**) and second (**b**) EOF mode of anthropogenic aerosol induced JJA precipitation changes (shadings, unit: mm day^{-1}, 9-year low-pass filtered) with explained variances marked on top right, and **e** their corresponding principal components (blue line denotes PC1 and red line denotes PC2, respectively) in CMIP6 Hist-Aer simulations. Vectors in **a** and **b** are the regressions of 850hPa winds anomalies to the corresponding PC1 and PC2 (unit: m s^{-1}, wind speed < 0.015 m s^{-1} omitted) with scale marked on top right. **c**, **d** are the regressions of 550nm AOD anomalies to the corresponding PC1 and PC2 (unit: 1)

response to the total AA forcing without considering the AA emissions changes in Europe. Effect of European AA emissions changes on EASM response can be captured by the second EOF mode of the low-frequency precipitation anomaly during 1950–2010 (Fig. 2b, e), which explains about 14.4% of the total variance. The PC2 of the EOF analysis increases first during 1950–1980 and then decreases during 1980–2010 (Fig. 2c). Regression of AOD to the PC2 indicates the important role of the European AA emissions changes in modulating this mode (Fig. 2d). For the spatial pattern of precipitation changes, unlike the uniform drying trend in the first mode, there is a contrast of the north–south dipole-like precipitation change in East Asia during distinct historical periods, with negative rainfall anomalies in northeast China and positive rainfall anomalies in Indo-China Peninsula during 1950–1980 and then the reversal during 1980–2010. The corresponding 850 hPa winds regressions also show cyclonic circulation anomaly over Europe in response to the increased aerosol emissions there during 1950–1980, while anti-cyclonic circulation anomaly during 1980–2010 resembles the declined European aerosol emissions. Moreover, the atmospheric circulation responses show divergent flow and northerlies in northern China mid-to-high latitudes and converge in Indo-China Peninsula and the adjacent maritime continent, pushing the climatological rain-belt to the south during 1950–1980 and backward to the north during 1980–2010. Therefore, the second EOF mode highlights the importance of the European AA emissions changes in governing the remote East Asian atmospheric circulation changes, leading to a response that is temporally varying (before and after 1980) and spatially contrasting (East China vs Indo-China Peninsula). This statistically derived result implies that the remote AA forcing effect counteracts the localized AA forcing in driving the EASM response during 1980–2010 but cooperates during 1950–1980.

The EOF analysis in the CMIP6 Hist-Aer simulations yields two distinct modes in AA induced EASM responses. Moreover, it is important to identify whether there is a distinguishable aerosol imprint in the EASM changes in the real world. To comprehensively assess the role of distinct AA emissions patterns in shaping the EASM responses, we regress the 9-year low-pass filtered precipitation and 850hPa wind anomalies in the CMIP6 Hist-Aer and historical all-forcing simulations, as well as in the observations onto the East Asian and European regional mean AOD changes (lines in Fig. 1a) during 1950–2010 (Fig. 3). Results in Fig. 3a and b resemble those in the EOF analysis very well, highlighting the two distinct modes in AA induced EASM responses. More importantly, in the all-forcing simulations, though with the influence of GHG forcing, there is still a significant rainfall decrease and weakening of EASM circulation in southeast Asia, resembling the EASM responses to the localized AA forcing (Fig. 3c). Besides, the EASM responses to

European AA emissions changes in all-forcing simulations (Fig. 3d) show marked similarities compared with that in the Hist-Aer simulations, featuring the south-north rain-belt shift in southeast Asia. The multi-model ensemble results in all-forcing simulations help to subtract the forced component of the EASM changes and highlight the important role of distinct AA emissions sources in driving the EASM changes. In the observations, the EASM change is a combination of externally forced signals and internal variabilities. Although the observed EASM responses to distinct AA emissions changes show complicated spatial patterns compared with the climate model results, the 9-year low-pass filtered regressions yet reveal the characters of both local (Fig. 3e) and remote (Fig. 3f) AA induced EASM changes. Instead of discrepancies between observations and climate models due to GHG forcing and internal climate variability, the individual contributions of local and remote AA forcing on the EASM changes are detectable in the real world.

4 Contrasting the AA induced EASM trends before and after the 1980s

4.1 Radiative flux and temperature response

To investigate the evolving EASM response to the distinct AA forcing spatial patterns and quantify their relative contributions to the historical EASM changes, we calculate the linear trends of TOA radiative flux, surface and tropospheric temperature in CMIP6 Hist-Aer simulations based on the multi-member and multi-model ensemble mean for three periods (1950–1980, 1980–2010, 1950–2010) separately.

During 1950–1980, when both Asian and European AA emissions increase (Fig. 1a, b), radiative flux change at the TOA shows robust negative centers in East Asia and Europe due to the "solar dimming" effect of the AA forcing (Fig. 4a). Consistent with the TOA radiative flux change, the surface temperature over the Eurasian continent shows significant cooling trend with the incoming solar radiation reflected by the AA (Fig. 4b). It is noteworthy that the effect of AA emissions is not only confined in the continent where they are emitted, but also can be transported downstream to the mid-latitude North Pacific by the southward shift of the westerly jet which is induced by the mid-latitude tropospheric cooling (Ming et al. 2011; Wang et al. 2016b; Diao et al. 2021). The negative radiative flux and cooling center east of Japan island may further influence the western North Pacific SST anomaly through the wind-evaporation-SST feedback (Xie 1996), and finally lead to the anomalous western Pacific subtropical high and corresponding EASM circulation anomaly via coupled ocean–atmosphere interaction processes (Chen et al. 2016).
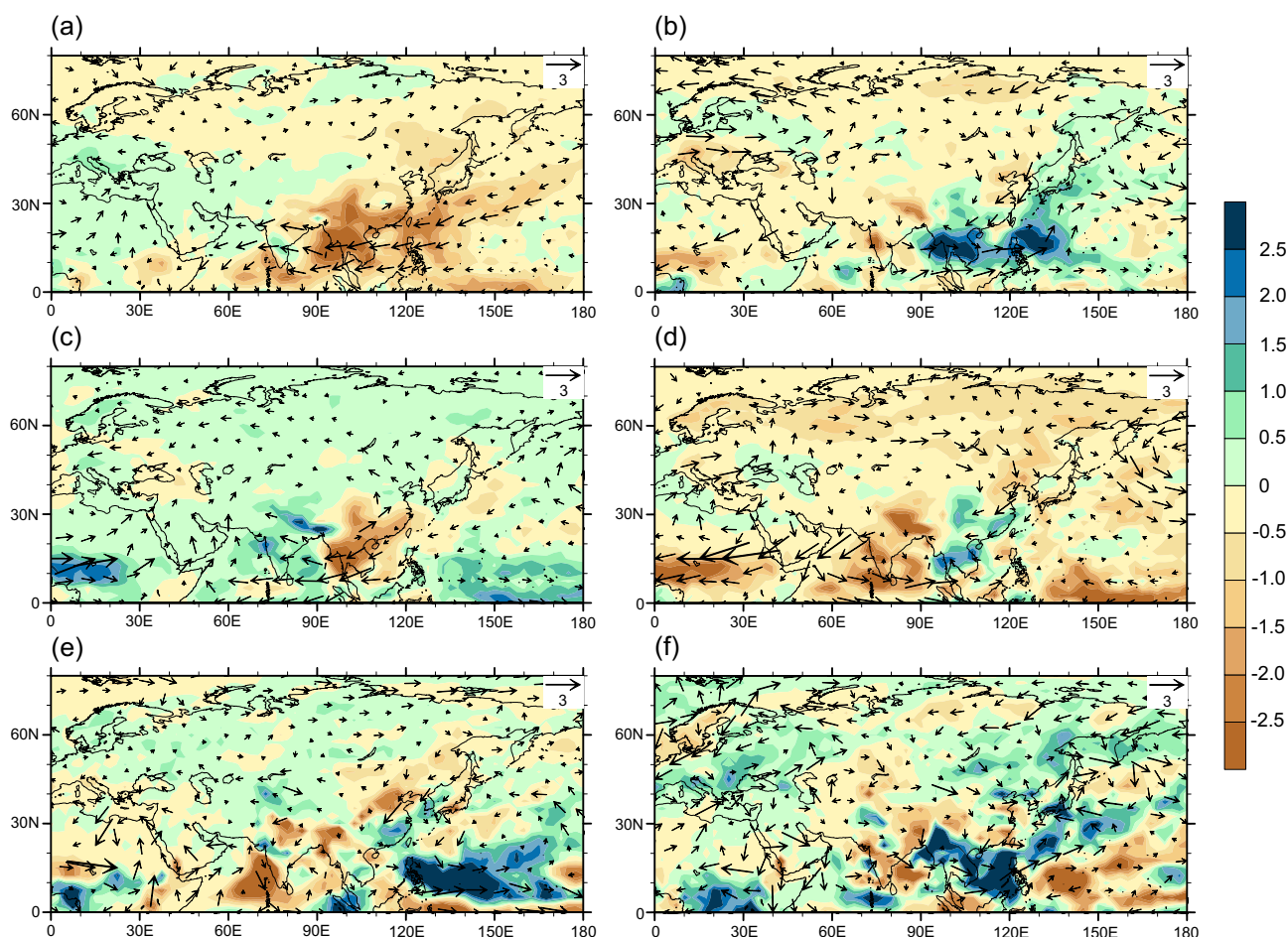
Fig. 3 Regressions of JJA precipitation (shadings, unit: mm day^{-1}) and 850 hPa wind (vectors, unit: m s^{-1}, wind speed < 0.3 m s^{-1} omitted, reference scale marked on top right) in **a**, **b** CMIP6 Hist-Aer simulation, **c**, **d** CMIP6 historical all-forcing simulation, and (e, f) ERA5 atmospheric reanalysis onto the East Asian (**a**, **c**, **e**) and European (**b**, **d**, **f**) regional mean AOD changes as shown in Fig. 1a during 1950–2010. A 9-year running average was applied to eliminate the high frequency signals before the regression analysis

After the 1980s, when the strict emission regulation was implemented in Europe, the AA emissions center was shifted from the western to the eastern hemisphere (Fig. 1a, c). Corresponding to the emissions changes, radiative flux at the TOA shows remarkable positive center in Europe and negative center in Asia (mainly in East Asia) (Fig. 4c). Correspondingly, the surface temperature in Europe increases and the warming trend is advected downstream to Eurasian continent by the climatological westerly jet. In contrast to previous period, over East Asia, the cooling due to the increasing AA emissions is confined to the land region and cannot be transported to the western North Pacific since the climatological westerly jet is weakened and shifted northward by the declined European AA emissions induced tropospheric warming during this period (see detailed discussion later) (Fig. 4d).

For the entire period of 1950–2010, the net change in European AA emissions is relatively small and the positive radiative flux and surface temperature warming anomaly are only centered in European continent, without the downstream effect found in the above two shorter separated periods (Fig. 4e, f). Over East Asia, the localized AA forcing leads to the regional cooling over land, thereby reduces the land-sea thermal contrast between the Asian continent and the adjacent oceans (Fig. 4f), which can further drive the atmospheric circulation anomaly.

In addition to the surface temperature anomaly, the two distinct AA forcing patterns also induce very different tropospheric temperature responses during the two historical periods. During 1950–1980, with the increase of AA emissions in the Northern Hemisphere, the tropospheric temperature shows a robust cooling trend with the maximum center located in both Europe and Asia (Fig. 5a). In contrast, during 1980–2010, the rapid decline of AA emissions from the WH lead to a warming anomaly in the mid-to-high latitude Northern Hemisphere while the
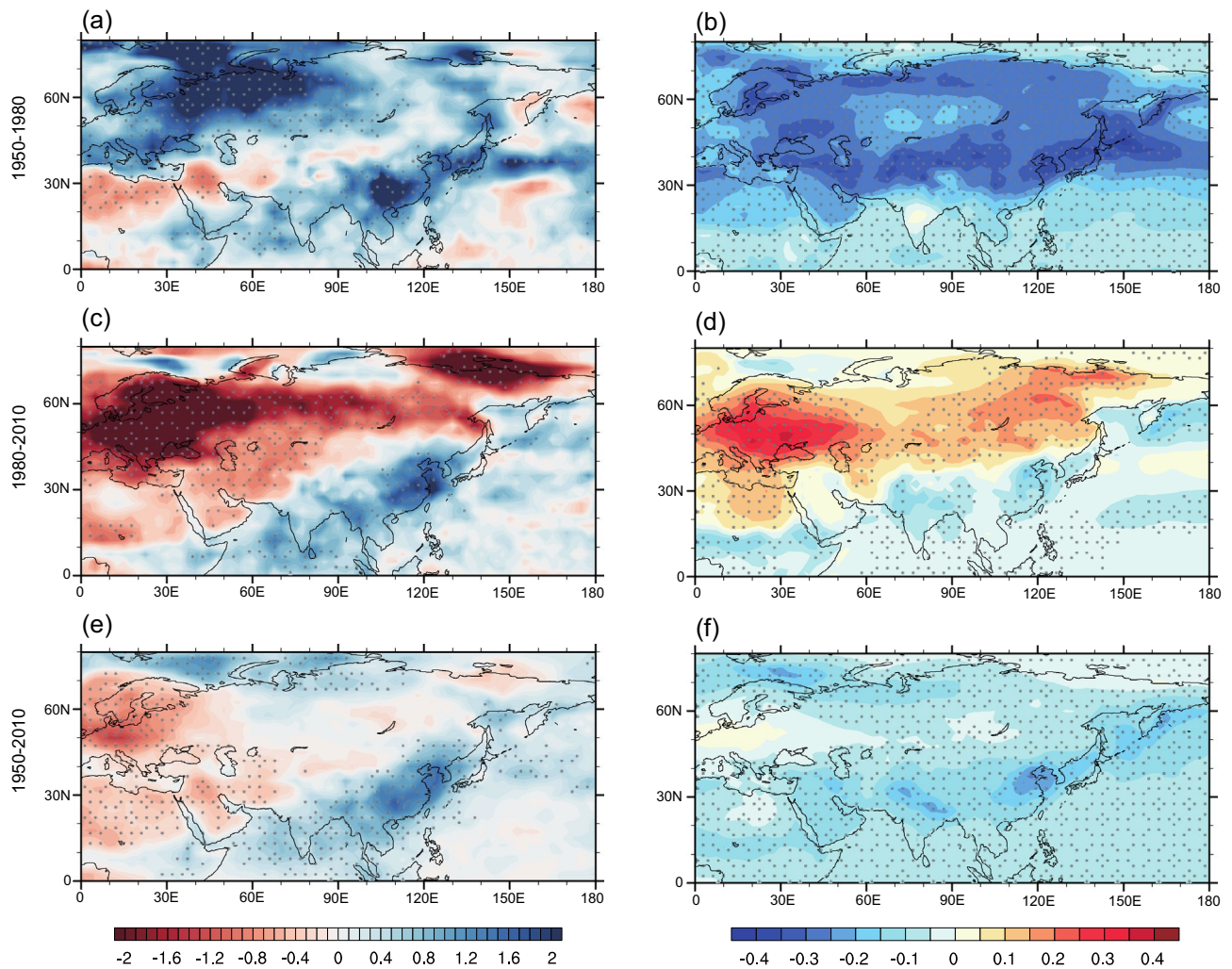
Fig. 4 Trends of JJA (**a**, **c**, **e**) net radiative flux in top of the atmosphere (unit: W m^{-2}/decade) and (**b**, **d**, **f**) surface temperature (unit: °C/decade) in CMIP6 Hist-Aer simulations during 1950–1980 (**a**, **b**), 1980–2010 (**c**, **d**), and 1950–2010 (**e**, **f**). Stippled regions indicate changes exceed 95% statistical confidence

increase of AA emissions from Asia results in the weak cooling trend in the mid-to-low latitude Northern Hemisphere (Fig. 5b). It is worth noting that the declining AA emissions from Europe can generate the local warming and also can lead to a significant warming anomaly downstream over the mid-to-high latitude Asian continent, which further implies the potential impact of European AA emissions changes on the EASM response through teleconnection. Again, if the AA induced response has been only examined for the entire period of 1950–2010, the tropospheric temperature anomaly is confined to the low-latitudes, which is consistent with the large-scale sea surface temperature response found in previous studies (Deser et al. 2020; Diao et al. 2021; Wang and Wen 2022). The distinctive tropospheric temperature patterns shown in Fig. 5 are important in driving the westerly jet anomalies through thermal wind balance and can also explain

the induced atmospheric teleconnections due to adiabatic heating anomaly. These are discussed next.

4.2 Atmospheric circulation response

Corresponding to the anomalous radiative flux and temperature responses in the surface and troposphere, atmospheric circulations show distinct responses to different AA forcing spatial patterns. Figure 6 shows the trends of zonally averaged temperature (color shading), westerly winds (contours), meridional and vertical velocities (vectors) in East Asia (100°E–140°E). Based on our previous study (Wang et al. 2019), the EASM response to AA forcing is largely due to the direct atmospheric response to radiative forcing without SST change, and to a lesser extent due to the AA induced North Pacific SST anomalies. During 1950–1980, the robust tropospheric cooling in East Asia centered around 45°N at
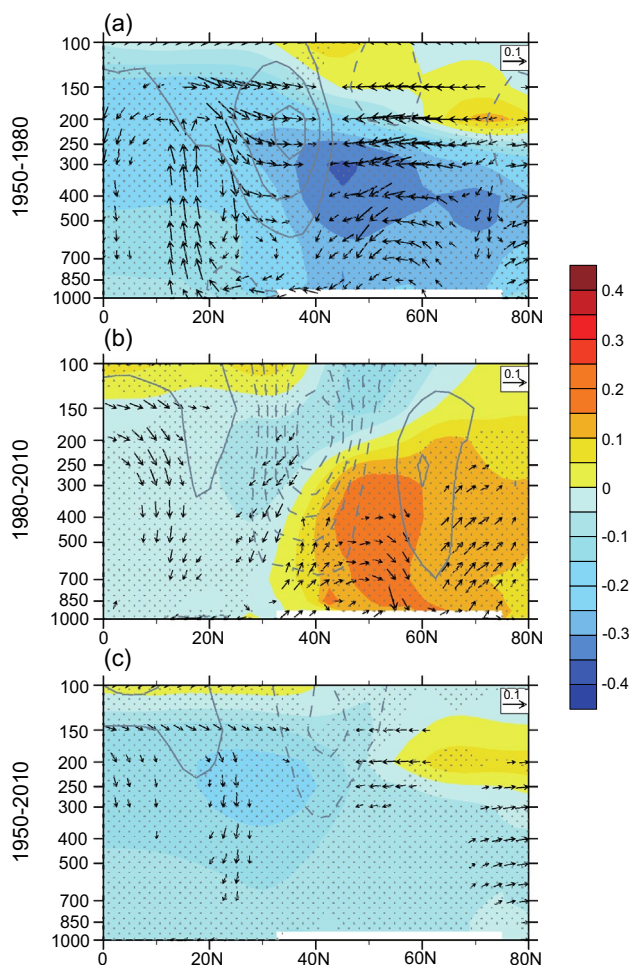
Fig. 5 Trends of JJA tropospheric temperature (200–850 hPa mean, unit: °C/decade) in CMIP6 Hist-Aer simulations during **a** 1950–1980, **b** 1980–2010, and **c** 1950–2010. Stippled regions indicate changes exceed 95% statistical confidence
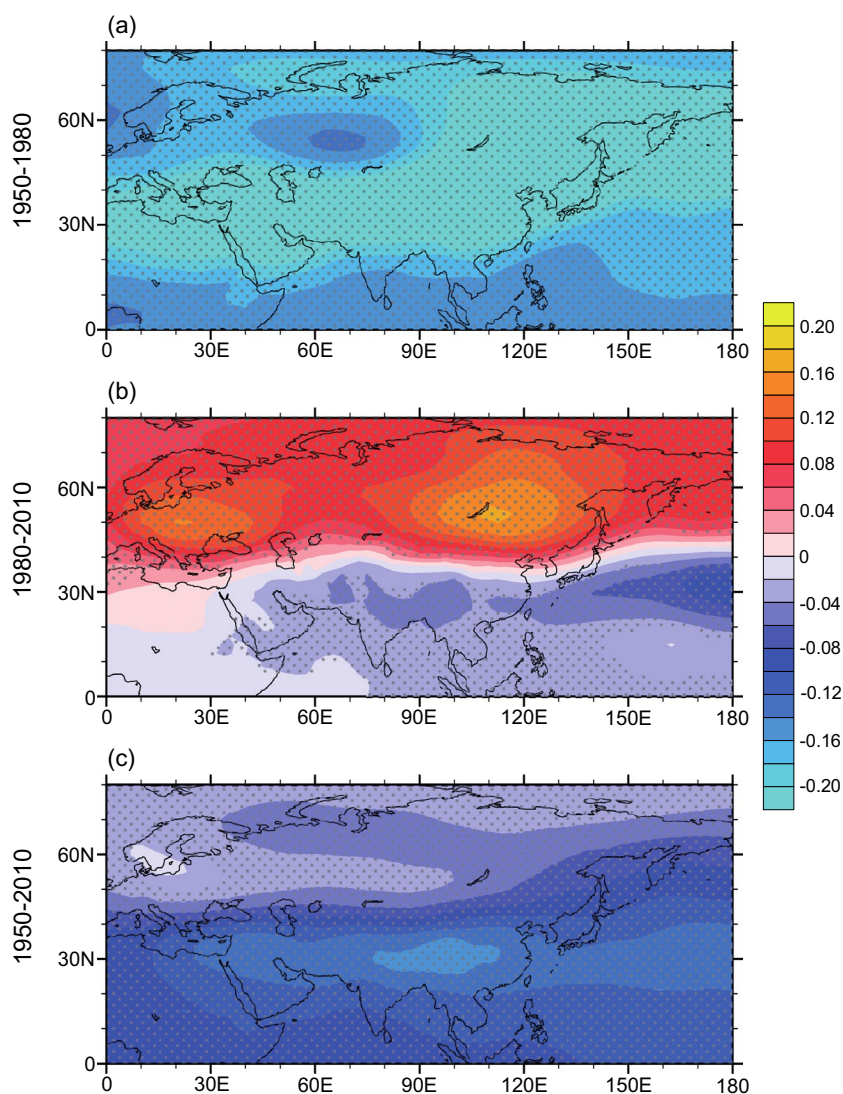
300 hPa (Fig. 6a), representing the joint effect of increase AA emissions from both East Asia and Europe. In maintaining the thermal wind balance, the deep cooling structure over the mid-latitude East Asia anchors a westerly acceleration to the south in the upper troposphere (centered around 35°N at 250 hPa). An anomalous local meridional overturning circulation develops with a sinking motion between 20°N and 50°N and a rising motion to the south of 20°N (Fig. 6a) and thus alleviates the climatological EASM circulation. During 1980–2010, by contrast, the mid-to-high latitude East Asian (north of 35°N) tropospheric temperature is warmed by the downstream effect of declined European AA emissions while the cooling induced by East Asian AA emissions is confined south of 30°N. In response to the warming anomaly, the climatological westerly is significantly weakened and shifted northward, and there is an anomalous sinking motion between 20°N and 30°N with anomalous rising motion north of 35°N (Fig. 6b). Comparison between

1950–1980 and 1980–2010 indicates that the European AA emissions changes may play a more important role than the localized East Asian AA emissions in shaping the EASM response by adjusting the thermal structure over Eurasian continent. This can further be illustrated by Fig. 6c, during 1950–2010 when the net European AA emissions change is relatively small, the East Asian AA induced tropospheric cooling center is lower in latitude than the first period and is centered around 30°N at 250hPa level. Moreover, the anomalous sinking motion is also weaker and more locally confined at 20°N–30°N (Fig. 6c), despite that the East Asian AA emissions increase more during 1950–2010 than that during 1950–1980 (Fig. 1a), suggesting a strong modulation role of European AA emissions (further highlighted in Sect. 5).

In addition to the tropospheric temperature and circulation changes, we also examine sea level pressure (SLP), precipitation and the 850 hPa winds (U and V) anomalies during the two distinct historical periods in response to

Fig. 6 Trends of JJA East Asian (100°E–140°E) zonal mean air temperature (shadings, unit: °C/decade), zonal wind speed (contours, unit: m s^{-1}/decade, 0.1 m s^{-1}/decade interval with 0 line omitted, solid contours indicate westerly wind), vertical (unit: 10^{-2} Pa s^{-1}/decade) and meridional (unit: m s^{-1}/decade) wind velocity (vectors, reference scale shown at the top right with values smaller than 0.03 omitted) in CMIP6 Hist-Aer simulations during **a** 1950–1980, **b** 1980–2010, and **c** 1950–2010. Stippled regions indicate the air temperature changes exceed 95% statistical confidence

different AA forcing patterns. During 1950–1980, consistent with the tropospheric cooling and the southward shifted westerly jet, the SLP shows a broad positive anomaly over the Eurasia continent (Fig. 7a), including the anti-cyclonic circulation anomaly as seen in the 850 hPa winds anomalies (Fig. 8a). The anomalous northeasterlies weaken the climatological EASM southwesterlies and lead to the drying trend of the EASM region by suppressing the atmospheric convections (Fig. 8a), with the spatial pattern largely consistent with the first EOF mode (Fig. 2a). In contrast, during 1980–2010, the robust negative SLP anomalies only exist in the mid-to-high latitude Eurasia continent in response to the declined European AA emissions and the resulting local tropospheric warming

(Fig. 7b). Note that there is no positive SLP anomaly in East Asia even though the local AA emissions keep increasing. The local and remote AA effects counteract with each other during this period, and only lead to a relatively weak EASM response (Fig. 8b). The positive/negative rainfall anomalies in northern/southern China with corresponding anomalous southerlies indicate that the remote AA's effect may have surprisingly overwhelmed the local AA's effect (Fig. 8b). The EASM response to the local AA forcing can be captured by the SLP, 850 hPa winds and precipitation changes during 1950–2010, because of the cancellation of the European AA emissions' trend. Corresponding to the increase of AA emissions from Asia, the tropospheric cooling anchors the high SLP anomaly and the weakened EASM circulation with robust drying trend in this period (Fig. 7c, and 8c).

To further evaluate to what extent the distinguishable AA emissions imprint in externally forced historical EASM changes at decadal time scales, we examine the corresponding precipitation and 850hPa winds changes in CMIP6 historical all-forcing simulations (Fig. 8d–f). Results show that during 1950–1980, the EASM changes in all-forcing results show similar EASM response patterns with that in the Hist-Aer simulations (spatial correlation of precipitation trend is 0.45), with weakened monsoon circulation and robust drying trend over East Asia (Fig. 8d). During 1950–1980, although the precipitation trend in all-forcing results is weakly correlates with that in the Hist-Aer simulations at 0.21, we can still see the enhanced EASM circulations with anomalous southerlies and corresponding north-positive south-negative precipitation trend in East Asia, highlighting the dominance of European AA emissions changes in shaping the EASM responses (Fig. 8e). In the whole periods of 1950–2010, the overall spatial correlation of precipitation changes between all-forcing and Hist-Aer simulation is 0.35. In East Asia, there is a drying trend over the mid-to-low latitudes and a weak wetting trend north of 35°N, with weak anomalous southerlies (Fig. 8f). This implies that the GHG induced warming may dominate over the AA forcing effect in the all-forcing simulations in the long-term change view. The comparison between all-forcing and Hist-Aer simulations highlights the importance of AA emissions changes in regulating the decadal EASM variations.

Inspections of the atmospheric structure, circulation, and EASM changes by contrasting the two distinct historical periods indicate that the remote AA forcing effects due to the European AA emissions changes may play a larger role than the local AA emissions from East Asia in shaping the historical decadal EASM evolutions. Therefore, it is of great importance to further reveal the dynamical mechanisms of how the European AA emissions modulate the atmospheric circulation and the EASM responses via the west-to-east atmospheric teleconnection.

Fig. 7 Trends of JJA sea level pressure (shadings, unit: Pa/decade) in CMIP6 Hist-Aer simulations during **a** 1950–1980, **b** 1980–2010, and **c** 1950–2010. Stippled regions indicate sea level pressure changes exceed 95% statistical confidence
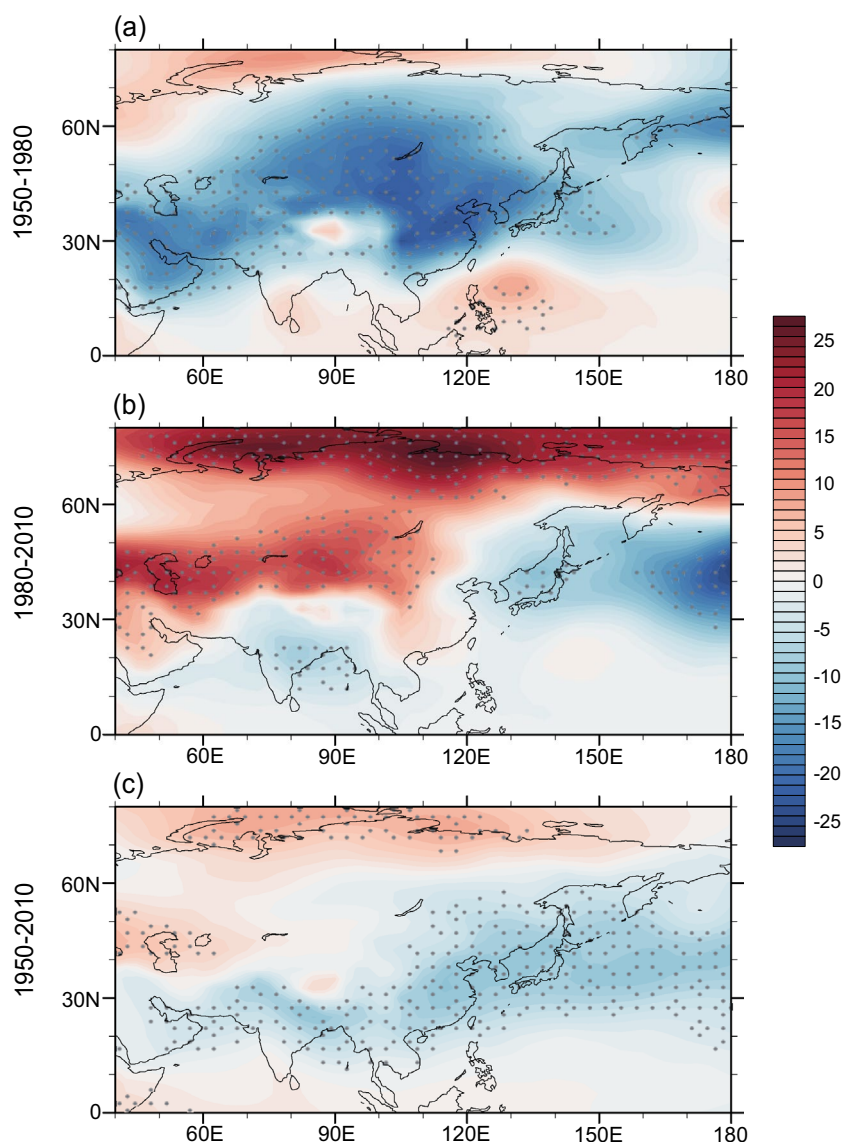

5 The dynamics of remote AA forcing in shaping the EASM response

5.1 CMIP6 results

For the Northern Hemisphere mid-latitude atmospheric circulation variations, previous studies revealed a circumglobal teleconnection pattern associated with the westerly jet stream that may influence the surface air temperature and rainfall anomalies in the continental region of Eurasia and East Asia in boreal summer (Ding and Wang 2005). Following this theoretical framework, we investigate whether the anomalous atmospheric heating induced by European AA emissions changes can generate similar atmospheric teleconnection responses that projects onto its downstream region in East Asia.

Figure 9a, c, and e show the point correlations between the tropospheric temperature (850hPa-200hPa mean) over Europe (0°–50°E; 40°N–60°N) and the 200 hPa geopotential height during 1950–1980, 1980–2010, and 1950–2010 in CMIP6 Hist-Aer simulations, respectively. Results indicate that in response to the European AA induced tropospheric temperature variations, the upper-tropospheric atmospheric circulation produces similar wave-train patterns downstream the heating source and induces robust geopotential height anomalies over Northeast Asia among the distinct historical periods, which may further modulate the EASM responses.

Besides, the 200hPa stream-function changes and the corresponding wave activity fluxes during distinct historical periods confirmed the remote influence of European AA emissions changes in shaping the atmospheric circulation responses in Eurasia continent and mid-to-high latitude East Asia. During 1950–1980, the increase of AA emissions from
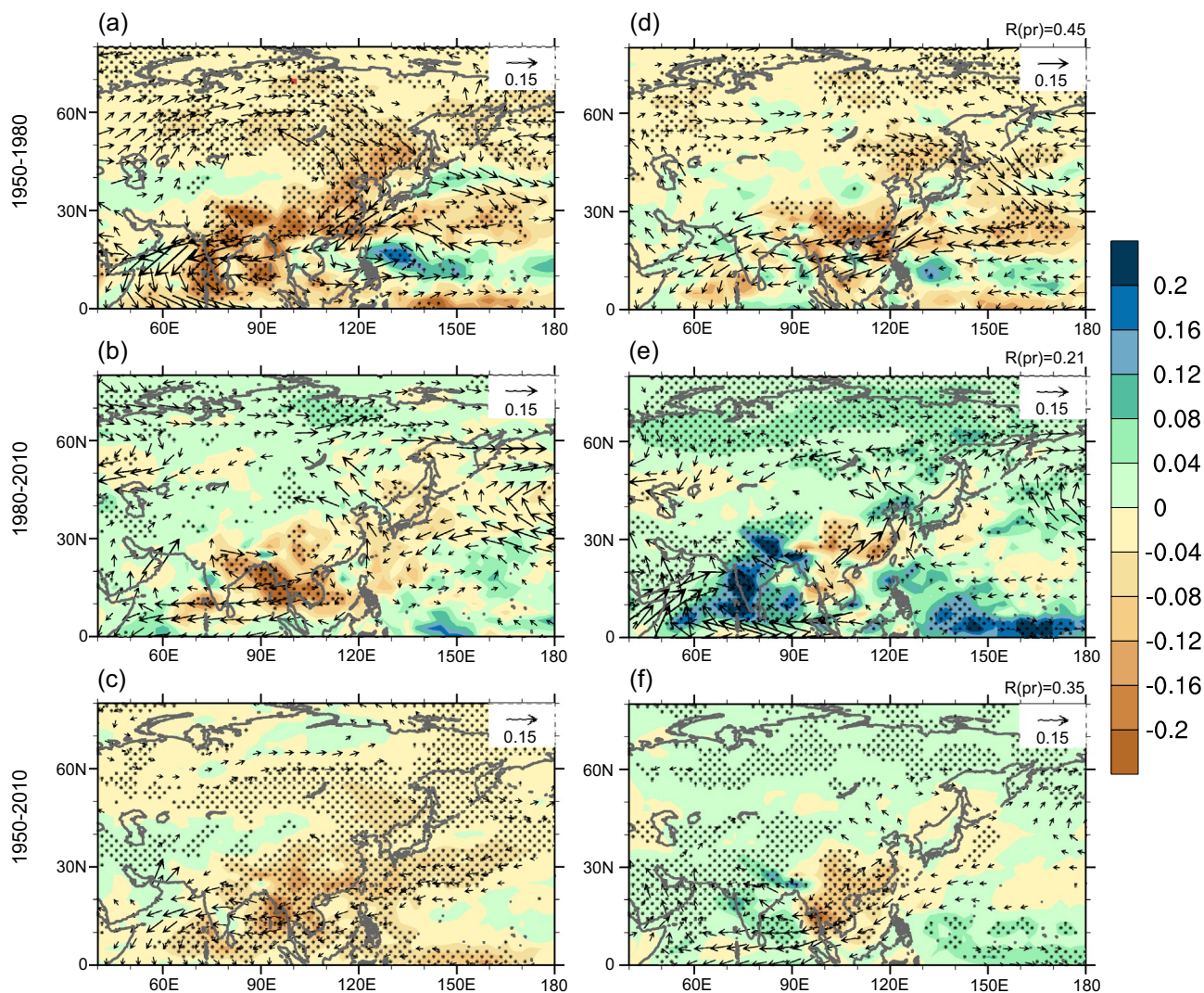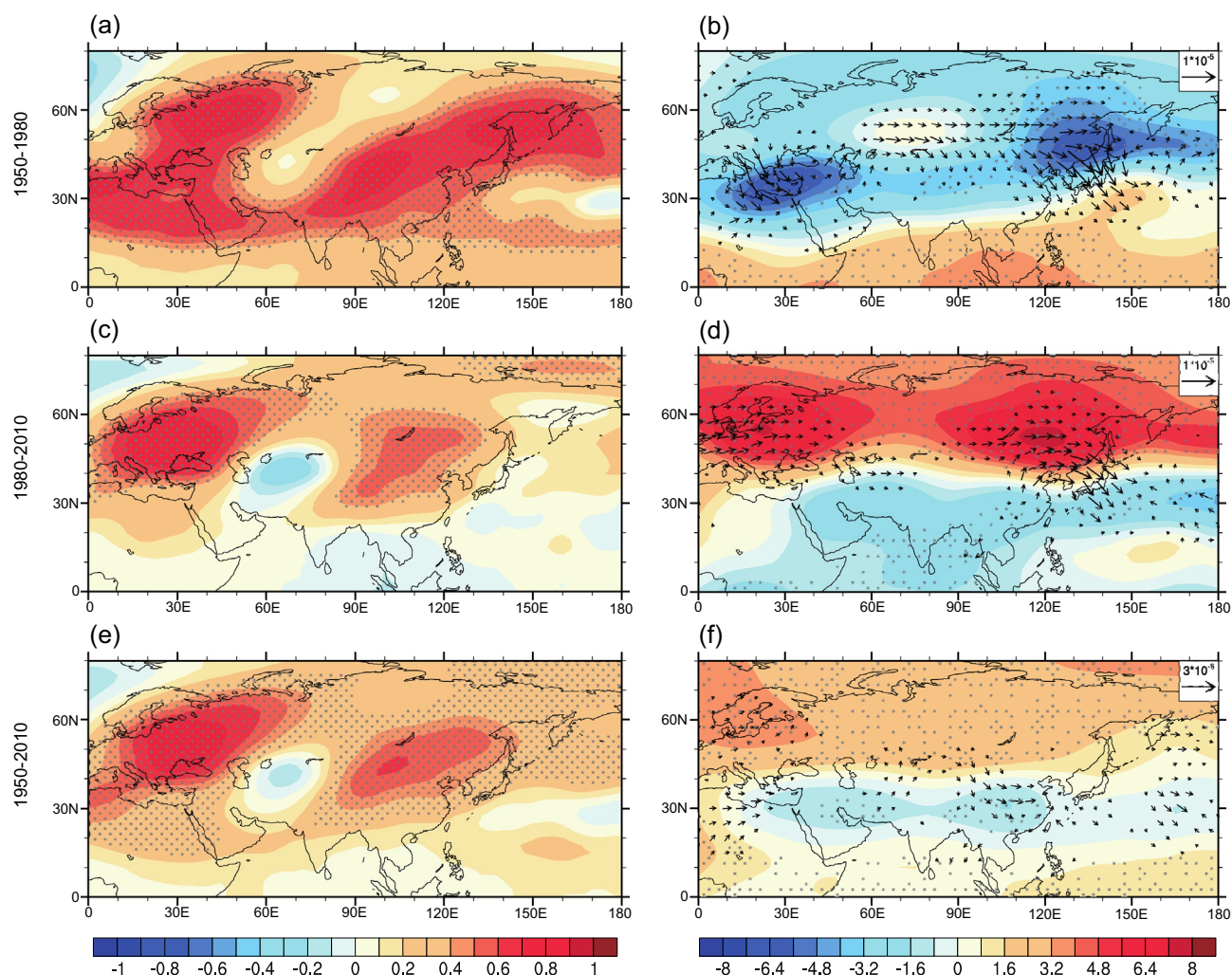
Fig. 8 Trends of JJA precipitation (shadings, unit: mm day^{-1}/decade) and 850hPa winds (vectors, unit: m s^{-1}/decade, reference scale shown at the top right with values smaller than 0.015 omitted) in **a**–**c** CMIP6 Hist-Aer simulations and **d**–**f** CMIP6 historical all-forcing simulations during **a**, **d** 1950–1980, **b**, **e** 1980–2010, and **c**, **f** 1950–2010.

Spatial correlations of precipitation trends between the all-forcing results and the aerosol single-forcing results are marked on top right in the right column. Stippled regions indicate precipitation changes exceed 95% statistical confidence

Europe generates the tropospheric cooling and lead to the negative stream-function anomaly, with the wave activity fluxes initiate from Europe and propagate eastward to Northeast Asia, resulting in the convergent flow there (Fig. 9b). In contrast, during 1980–2010, the anomalous divergent flow over Northeast Asia is also generated remotely by the declined AA emissions from Europe, while the local effect due to the increase of AA emissions from East Asia is confined in the mid-to-low latitude regions (Fig. 9d). During 1950–2010, when the net European AA emissions change is largely balanced, the mid-latitude atmospheric teleconnection disappears and the East Asian AA induced atmospheric circulation response is restricted to the emission source (Fig. 9f).

The atmospheric teleconnection analysis in Fig. 9 clearly demonstrates the important role of the European AA emissions changes in modulating the EASM circulation anomalies, especially in Northeast Asia. The anomalous convergent flow in the upper troposphere in East Asia during 1950–1980 is generated jointly by both the European and the Asian AA emissions increases, which results in the anomalous descent around 45°N (Fig. 6a) and leads to the corresponding weakening of the EASM with anomalous northerlies (Fig. 8a). However, during 1980–2010, albeit the East Asian AA emissions increase favors the weakening of EASM, the divergent flow in the upper troposphere over northeast Asia leads to the anomalous ascent around 40°N (Fig. 6b). This vertical ascent results in the anomalous southerlies in the lower

Fig. 9 **a**, **c**, **e** Spatial correlation between JJA 200hPa geopotential height and European (40°N–60°N, 0–50°E) regional mean tropospheric temperature (200hPa-850hPa mean) anomalies. **b**, **d**, **f** are the trends of JJA 200hPa stream-function (shadings, unit: 1×10^5 m^2 s^{-1}/ decade) and wave-activity flux (vectors, unit: m^2 s^{-2}/decade, refer-ence scale shown at the top right with values smaller than 1×10^{-6} in **b**, **d** and 3×10^{-7} in **f** omitted) in CMIP6 Hist-Aer simulations during 1950–1980 (**a**, **b**), 1980–2010 (**c**, **d**), and 1950–2010 (**e**, **f**). Stippled regions indicate the spatial correlation and stream-function changes exceed 95% statistical confidence

troposphere causing a drying trend in Southeast Asia and a wetting trend in Northeast Asia, masking the local cooling effect of the increase AA emissions from East Asia (Fig. 8b). Therefore, our results demonstrate that the AA induced mid-to-high latitude EASM response is dominated by the remote European AA emissions changes, instead of the local AA emissions changes in Asia. This identification of non-Asian contribution advances our previous understandings of the AA induced EASM response mechanisms (Li et al. 2016).

5.2 WH experiments results

Since the CMIP6 analysis on the remote influence of European AA emissions changes on the EASM response is based on statistical regression and linear trend approaches,

we further validate the causal relationship by using the dedicated WH experiments branched from the CESM1-LENS and the Fix_FF1920 climate model simulations. By differencing the WH experiments results and the CESM1-LENS results, the European AA emissions changes during 1980–2010 can be well captured, showing a robust negative 550nm AOD trend centered in Europe, with little change in East Asia (Fig. 10a). Since the North American AA emissions changes are smaller than Europe (Diao et al. 2021; Wang et al. 2021b), the WH experiments yield the response of EASM to European AA emissions changes very well without the influence of Asian AA emissions changes. In response to the declined AA emissions from Europe, the surface temperature shows significant warming trend in Europe and its downstream region (Fig. 10b),
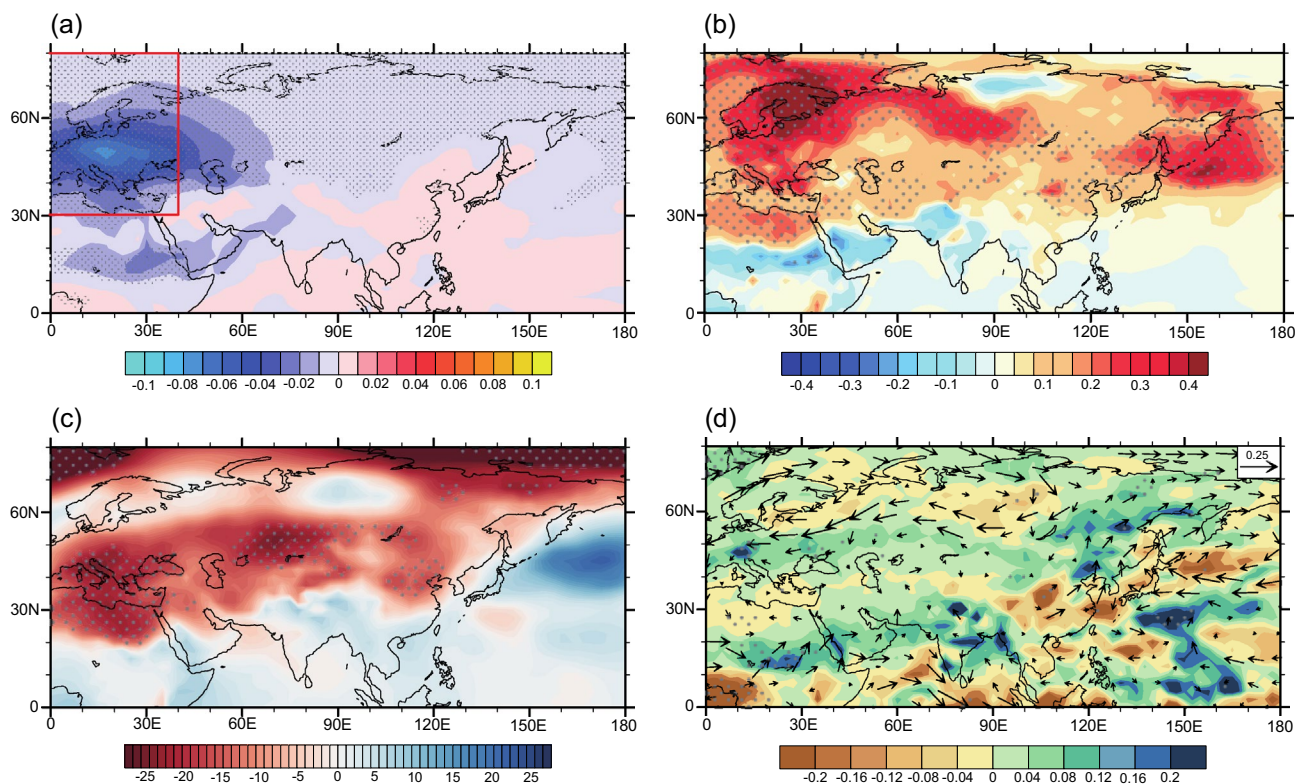
Fig. 10 Trends of JJA **a** Aerosol Optical Depth (ambient aerosol optical thickness at 550nm; unit: 1/decade), **b** surface temperature (unit: °C/decade), **c** sea level pressure (unit: Pa/decade), **d** precipitation (shadings, unit: mm day^{-1}/decade) and 850hPa winds (vectors, unit: m s^{-1}/decade, reference scale shown at the top right with values smaller than 0.05 omitted) in CESM1 WH experiments dur-ing 1980–2010. Stippled regions indicate the changes (precipitation change in **d**) exceed 95% statistical confidence. The area enclosed by the red lines in **a** denotes the geographic boundary of European sector (30°N–80°N, 10°W–40°E) where the AA emissions are fixed in the WH experiments

with corresponding negative SLP changes in mid-to-high latitude Eurasia and Northeast Asia (Fig. 10c). For the 850 hPa winds and precipitation changes in EASM region (Fig. 10d), it resembles the results in CMIP6 Hist-Aer simulations (Fig. 8b), with anomalous southerlies that strengthens the climatological EASM and the rainfall

shows a south-drought north-flood pattern due to the atmospheric circulation changes.

Moreover, in the upper troposphere, the abovementioned atmospheric teleconnection generated by the European tropospheric warming (Fig. 9d) can also be reproduced by the WH experiments (Fig. 11), with similar anomalous

Fig. 11 Trends of JJA 200hPa stream-function (shadings, unit: 1×10^5 m^2 s^{-1}/decade) and wave-activity flux (vectors, unit: m^2 s^{-2}/decade, reference scale shown at the top right with values smaller than 3×10^{-6} m^2 s^{-2}/decade omitted) in CESM1 WH experiments during 1980–2010. Stippled regions indicate the stream-function changes exceed 95% statistical confidence
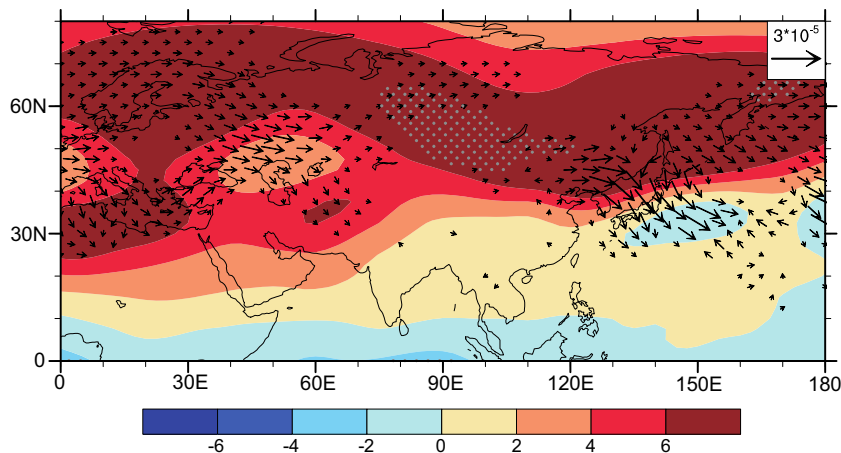
stream-functions (color shading) and stationary waves (vectors) propagating from Europe to Northeast Asia. The WH experiments exclude the effect of Asian AA emissions changes in the CMIP6 Hist-Aer simulations, and highlight the importance of the European AA emissions changes in modulating the EASM monsoon circulation and precipitation changes since the 1980s.

6 Summary and discussion

As a major and uncertain external radiative forcing of climate change, AA's effect masks a considerable fraction of the GHG induced warming since the industrial revolution. For East Asia, where AA emissions are concentrated, significant regional climate responses have been documented previously, especially the EASM changes that have devastating impacts on the social and economic developments. Unlike the well-mixed GHGs, the spatial and temporal evolutions of AA forcing vary rapidly due to heterogeneous emission sources and short atmospheric resident time, posing the need to better understand their role in modulating the decadal regional climate change.

Since the mid-twentieth century, AA emissions shifted from western to eastern hemisphere, inducing pronounced large-scale climate responses such as the northward shifts of tropical rain-belt and the La Niña like tropical SST responses (Deser et al. 2020; Qin et al. 2020; Kang et al. 2020; Diao et al. 2021; Wang and Wen 2022). However, how the decadal EASM may respond to the spatial and temporal evolutions of AA forcing since the mid-twentieth century remained to be thoroughly investigated. Here, we demonstrate the role of AA emissions changes over both Europe and East Asia in shaping the decadal EASM changes by contrasting distinct historical periods, advancing our previous understandings of AA's effect on regional climate system.

Using the CMIP6 Hist-Aer simulations, we firstly extract the principal components of the EASM precipitation and circulation changes during 1950–2010. To the first order, the leading EOF mode captures the effect of the long-term monotonic increase of AA emissions from East Asia, with a marked weakened EASM circulation and a robust drying trend over East Asia. European AA emissions had gone through an increase trend during 1950–1980 and a decrease trend during 1980–2010, effectively leading to the shift of AA emissions centers from Europe to East Asia since the 1980s. We identify this shift mode as the second EOF mode of the Eurasia precipitation and circulation analysis. The reversal of AA emissions trends over Europe not only feature the European regional temperature and circulation changes, but also weaken the EASM precipitation and circulation during 1950–1980 but intensify them during 1980–2010. Besides, these two distinct modes of AA induced EASM

changes are detectable in both CMIP6 historical all-forcing simulations and observations, though with influences from either GHG forcing or internal climate variability.

More systematically, we examined three different periods separately to quantify the time-evolving contributions to the EASM responses from distinct spatial patterns of AA forcing. In the first period during 1950–1980, both the AA emissions from Europe and East Asia increase significantly. Due to the scattering and reflecting effect of aerosol particles, less incoming solar radiation in the troposphere leads to the tropospheric cooling in the Eurasia continent, accompanying by the southward shift of the westerly jet duo to thermal wind balance, and resulting in a robust weakening of EASM circulation and drying trend in East Asia. During 1980–2010, although there was a fast increase in AA emissions from East Asia, the EASM is intensified by anomalous southerlies due to European AA forcing reversal and indeed the precipitation increase in Northeast Asia, largely counterbalancing the local AA forcing effect. The net European AA emissions changed little during 1950–2010 and did not exert remote influence over Asia; and as a result, the EASM response resembles the previous understandings of the overall AA induced long-term Asian summer monsoon response (Wang et al. 2019).

Diagnostic analysis of tropospheric temperature and circulation responses indicate that the European AA emissions changes play a more important role than the local AA forcing in shaping the EASM response at decadal time scale, for both 1950–1980 and 1980–2010. Both the CMIP6 Hist-Aer simulation and the dedicated perturbation simulations (WH experiments) confirm that the tropospheric heating anomaly due to the changes in AA emissions from Europe can induce an atmospheric teleconnection emitting from the heating anomaly and propagation downstream the westerly jet to Northeast Asia, generating the EASM responses remotely.

Our findings advance previous understandings of the AA induced EASM changes by providing a spatially and temporally varying viewpoint, and by highlighting the important role of AA emissions changes in Europe in modulating the decadal EASM anomalies. The role of non-local forcing can be vastly omitted if the analysis is done only for the longer period (1950–2010), as in many previous studies (Song et al. 2014; Li et al. 2015; Chen et al. 2016; Wang et al. 2019), due to the phase transition of European AA emissions. Note that such a phase transition may have started in East Asia since the 2010s and may occur in South Asia in the next few decades, leading to the complexity of interpreting AA's role in regional climate change. Since China's implementation of air pollution prevention and control action in 2013, a dipole forcing pattern has been found between the South and East Asia with AA emissions from East Asia greatly reduced, and South Asian emissions continuing to increase (Zheng et al. 2018; Samset et al. 2019). Some recent studies have

shown that this AA forcing pattern inside Asia has contributed to the observed anomalies of the EASM precipitation in East China (Wang et al. 2021a; Wang et al. 2022; Liu et al. 2022). However, how this dipole pattern will modulate the regional direct atmospheric responses as well as the coupled ocean–atmosphere responses in Northwest Pacific and Indian Ocean remain to be investigated in the future.

Data availability The Phase 6 of Coupled Model Intercomparison Project (CMIP6) climate model simulations can be obtained via the Earth System Grid Federation (ESGF) nodes, https://esgf-node.llnl. gov/search/cmip6/. The CESM1 Large Ensemble data sets are publicly available from https://www.cesm.ucar.edu/projects/community-projects/LENS/data-sets.html. The CESM1 "Single Forcing" Large Ensemble data sets are publicly available from https://www.cesm. ucar.edu/working_groups/CVC/simulations/cesm1-single_forcing_le. html. The outputs for WH regional single-forcing large-ensemble (Fix_WestFF1920) are available on the National Center for Atmospheric Research (NCAR) Campaign Storage file system under /glade/campaign/univ/utam0012/CESM11-LEN-Reg/ and can also be accessed via the NCAR Data Sharing Service Endpoint on Globus upon request to the authors. The fifth generation European Centre for Medium-Range Weather Forecasts atmospheric reanalysis (ERA5) are publicly available from https://www.ecmwf.int/en/forecasts/dataset/ecmwf-reanalysis-v5.

Code availability Scripts for analyzing the data will be available from the corresponding author upon reasonable request.

Declarations

Conflict of interest The authors have no competing interests to declare that are relevant to the content of this article.

References

Bellouin N et al (2020) Bounding global aerosol radiative forcing of climate change. Rev Geophys 58:e2019RG000660. https://doi.org/10.1029/2019RG000660

Bollasina MA, Ming Y, Ramaswamy V (2011) Anthropogenic aerosols and the weakening of the South Asian summer monsoon. Science 334(6055):502–505. https://doi.org/10.1126/science.1204994

Chen JP, Chen IJ, Tsai IC (2016) Dynamic feedback of aerosol effects on the East Asian summer monsoon. J Clim 29:6137–6149. https://doi.org/10.1175/JCLI-D-15-0758.1

Choi W, Kim KY (2019) Summertime variability of the western North Pacific subtropical high and its synoptic influences on the East Asian weather. Sci Rep 9:7865. https://doi.org/10.1038/s41598-019-44414-w

Deser C et al (2020) Isolating the evolving contributions of anthropogenic aerosols and greenhouse gases: a new CESM1 large ensemble community resource. J Clim 33(18):7835–7858. https://doi.org/10.1175/JCLI-D-20-0123.1

Diao C, Xu Y, Xie SP (2021) Anthropogenic aerosol effects on tropospheric circulation and sea surface temperature (1980–2020): separating the role of zonally asymmetric forcings. Atmos Chem Phys 21:18499–18518. https://doi.org/10.5194/acp-21-18499-2021

Ding Y, Chan JCL (2005) The East Asian summer monsoon: an overview. Meteorol Atmos Phys 89:117–142. https://doi.org/10.1007/s00703-005-0125-z

Ding Q, Wang B (2005) Circumglobal teleconnection in the Northern Hemisphere summer. J Clim 18(17):3483–3505. https://doi.org/10.1175/JCLI3473.1

Dong B, Sutton RT, Highwood EJ, Wilcox LJ (2016) Preferred response of the East Asian summer monsoon to local and nonlocal anthropogenic sulphur dioxide emissions. Clim Dyn 46:1733–1751. https://doi.org/10.1007/s00382-015-2671-5

Dong B, Sutton RT, Shaffrey L, Harvey B (2022) Recent decadal weakening of the summer Eurasian westerly jet attributable to anthropogenic aerosol emissions. Nat Commun 13(1):1148. https://doi.org/10.1038/s41467-022-28816-5

Eyring V, Bony S, Meehl GA, Senior CA, Stevens B, Stouffer RJ, Taylor KE (2016) Overview of the coupled model intercomparison project phase 6 (CMIP6) experimental design and organization. Geosci Model Dev 9(5):1937–1958. https://doi.org/10.5194/gmd-9-1937-2016

Feng J, Wang L, Chen W (2014) How does the east asian summer monsoon behave in the decaying phase of el niño during different PDO phases. J Clim 27:2682–2698. https://doi.org/10.1175/JCLI-D-13-00015.1

Ganguly D, Rasch PJ, Wang H, Yoon JH (2012) Fast and slow responses of the South Asian monsoon system to anthropogenic aerosols. Geophys Res Lett 39(18):L18804. https://doi.org/10.1029/2012GL053043

Gong DY, Ho CH (2002) Shift in the summer rainfall over the Yangtze River valley in the late 1970s. Geophys Res Lett 29:78–81. https://doi.org/10.1029/2001GL014523

Hersbach H et al (2020) The ERA5 global reanalysis. Q J R Meteorol Soc 146:1999–2049. https://doi.org/10.1002/qj.3803

Kang SM, Held IM, Frierson DMW, Zhao M (2008) The response of the ITCZ to extratropical thermal forcing: idealized slab-ocean experiments with a GCM. J Clim 21(14):3521–3532. https://doi.org/10.1175/2007JCLI2146.1

Kang SM, Xie SP, Shin Y, Kim H, Hwang YT, Stuecker MF, Xiang B, Hawcroft M (2020) Walker circulation response to extratropical radiative forcing. Sci Adv 6(47):eabd021. https://doi.org/10.1126/sciadv.abd3021

Kay JE et al (2015) The community earth system model (CESM) large ensemble project: a community resource for studying climate change in the presence of internal climate variability. Bull Am Meteor Soc 96(8):1333–1349. https://doi.org/10.1175/BAMS-D-13-00255.1

Kitoh A, Endo H, Kumar KK, Cavalcanti IFA, Goswami P, Zhou T (2013) Monsoons in a changing world: a regional perspective in

a global context. J Geophys Res Atmos 118:3053–3065. https://doi.org/10.1002/jgrd.50258

Lee JY, Wang B (2014) Future change of global monsoon in the CMIP5. Clim Dyn 42(1–2):101–119. https://doi.org/10.1007/s00382-012-1564-0

Lei Y, Hoskins B, Slingo J (2011) Exploring the interplay between natural decadal variability and anthropogenic climate change in summer rainfall over China. Part I: observational evidence. J Clim 24:4584–4599. https://doi.org/10.1175/2010JCLI3794.1

Li X, Ting M, Li C, Henderson N (2015) Mechanisms of Asian summer monsoon changes in response to anthropogenic forcing in CMIP5 models. J Clim 28(10):4107–4125. https://doi.org/10.1175/JCLI-D-14-00559.1

Li Z et al (2016) Aerosol and monsoon climate interactions over Asia. Rev Geophys 54:866–929. https://doi.org/10.1002/2015RG000500

Li X, Ting M, Lee DE (2018) Fast adjustment of the Asian summer monsoon to anthropogenic aerosols. Geophys Res Lett 45(2):1001–1010. https://doi.org/10.1002/2017GL076667

Li X, Ting M, You Y, Lee DE, Westervelt DM, Ming Y (2020) South Asian summer monsoon response to aerosol-forced sea surface temperatures. Geophys Res Lett 47(1):e2019GL085329. https://doi.org/10.1029/2019GL085329

Lin L, Xu Y, Wang Z, Diao C, Dong W, Xie SP (2018) Changes in extreme rainfall over india and china attributed to regional aerosol-cloud interaction during the late 20th century rapid industrialization. Geophys Res Lett 45(15):7857–7865. https://doi.org/10.1029/2018GL078308

Liu J et al (2017) Aerosol-weakened summer monsoons decrease lake fertilization on the Chinese Loess Plateau. Nat Clim Change 7:190–194. https://doi.org/10.1038/nclimate3220

Liu L et al (2018) A pdrmip multimodel study on the impacts of regional aerosol forcings on global and regional precipitation. J Clim 31(11):4429–4447. https://doi.org/10.1175/JCLI-D-17-0439.1

Liu C, Yang Y, Wang H, Ren L, Wei J, Wang P, Liao H (2022) Influence of spatial dipole pattern in Asian aerosol changes on East Asian summer monsoon. J Clim. https://doi.org/10.1175/JCLI-D-22-0335.1

Ma S et al (2017) Detectable anthropogenic shift toward heavy precipitation over Eastern China. J Clim 30:1381–1396. https://doi.org/10.1175/JCLI-D-16-0311.1

Ming Y, Ramaswamy V, Chen G (2011) A model investigation of aerosol-induced changes in boreal winter extratropical circulation. J Clim 24:6077–6091. https://doi.org/10.1175/2011JCLI4111.1

Mu J, Wang Z (2021) Responses of the East Asian summer monsoon to aerosol forcing in CMIP5 models: the role of upper-tropospheric temperature change. Int J Climatol 41(3):1555–1570. https://doi.org/10.1002/joc.6887

Myhre G et al (2013) Anthropogenic and natural radiative forcing. In: Stocker TF et al (eds) Climate change 2013: the physical science basis. Cambridge University Press, Cambridge, New York, pp 659–740

Oudar T, Kushner PJ, Fyfe JC, Sigmond M (2018) No impact of anthropogenic aerosols on early 21st century global temperature trends in a large initial-condition ensemble. Geophys Res Lett 45(17):9245–9252. https://doi.org/10.1029/2018GL078841

Pascoe C, Lawrence BN, Guilyardi E, Juckes M, Taylor KE (2019) Designing and documenting experiments in CMIP6. Geosci Model Dev Discuss. https://doi.org/10.5194/gmd-2019-98

Qian Y, Flanner MG, Leung LR, Wang W (2011) Sensitivity studies on the impacts of Tibetan Plateau snowpack pollution on the Asian hydrological cycle and monsoon climate. Atmos Chem Phys 11(5):1929–1948. https://doi.org/10.5194/acp-11-1929-2011

Qin M, Dai A, Hua W (2020) Aerosol-forced multidecadal variations across all ocean basins in models and observations since 1920. Sci Adv 6(29):eabb0425. https://doi.org/10.1126/sciadv.abb0425

Samset BH, Lund MT, Bollasina M, Myhre G, Wilcox L (2019) Emerging Asian aerosol patterns. Nat Geosci 12(8):582–584. https://doi.org/10.1038/s41561-019-0424-5

Singh D (2016) Tug of war on rainfall changes. Nat Clim Chang 6(1):20–22. https://doi.org/10.1038/nclimate2901

Song F, Zhou T, Qian Y (2014) Response of East Asian summer monsoon to natural and anthropogenic forcings in the 17 latest CMIP5 models. Geophys Res Lett 41(2):596–603. https://doi.org/10.1002/2013GL058705

Takaya K, Nakamura H (2001) A formulation of a phase-independent wave-activity flux for stationary and migratory quasigeostrophic eddies on a zonally varying basic flow. J Atmos Sci 58:608–627. https://doi.org/10.1175/1520-0469(2001)058%3c0608:AFOAPI%3e2.0.CO;2

Trenberth K (2011) Changes in precipitation with climate change. Clim Res 47(1–2):123–138. https://doi.org/10.3354/cr00953

Undorf S, Bollasina MA, Hegerl GC (2018) Impacts of the 1900–1974 increase in anthropogenic aerosol emissions from North America and Europe on Eurasian summer climate. J Clim 31(20):8381–8399. https://doi.org/10.1175/JCLI-D-17-0850.1

Wang H, Wen YJ (2022) Climate response to the spatial and temporal evolutions of anthropogenic aerosol forcing. Clim Dyn 59:1579–1595. https://doi.org/10.1007/s00382-021-06059-2

Wang Y, Jiang JH, Su H (2015) Atmospheric responses to the redistribution of anthropogenic aerosols. J Geophys Res Atmos 120(18):9625–9641. https://doi.org/10.1002/2015JD023665

Wang H, Xie SP, Tokinaga H, Liu Q, Kosaka Y (2016a) Detecting cross-equatorial wind change as a fingerprint of climate response to anthropogenic aerosol forcing. Geophys Res Lett 43(7):3444–3450. https://doi.org/10.1002/2016GL068521

Wang H, Xie SP, Liu Q (2016b) Comparison of climate response to anthropogenic aerosol versus greenhouse gas forcing: distinct patterns. J Clim 29(14):5175–5188. https://doi.org/10.1175/JCLI-D-16-0106.1

Wang Z, Lin L, Yang M, Xu Y, Li J (2017) Disentangling fast and slow responses of the East Asian summer monsoon to reflecting and absorbing aerosol forcings. Atmos Chem Phys 17:11075–11088. https://doi.org/10.5194/acp-17-11075-2017

Wang H, Xie SP, Kosaka Y, Liu Q, Du Y (2019) Dynamics of Asian Summer monsoon response to anthropogenic aerosol forcing. J Clim 32(3):843–858. https://doi.org/10.1175/JCLI-D-18-0386.1

Wang Z, Mu J, Yang M, Yu X (2020) Reexamining the mechanisms of East Asian summer monsoon changes in response to non-East Asian anthropogenic aerosol forcing. J Clim 33(8):2929–2944. https://doi.org/10.1175/JCLI-D-19-0550.1

Wang Z et al (2021a) Incorrect Asian aerosols affecting the attribution and projection of regional climate change in CMIP6 models. NPJ Clim Atmos Sci 4:2. https://doi.org/10.1038/s41612-020-00159-2

Wang Z, Feng J, Diao C, Li Y, Lin L, Xu Y (2021b) Reduction in European anthropogenic aerosols and the weather conditions conducive to $PM_{2.5}$ pollution in North China: a potential global teleconnection pathway. Environ Res Lett 16:104054. https://doi.org/10.1088/1748-9326/ac269d

Wang C, Wang Z, Lei Y, Zhang H, Che H, Zhang X (2022) Differences in East Asian summer monsoon responses to Asian aerosol forcing under different emission inventories. Adv Clim Chang Res 13(3):309–322. https://doi.org/10.1016/j.accre.2022.02.008

Westervelt DM et al (2018) Connecting regional aerosol emissions reductions to local and remote precipitation responses. Atmos Chem Phys 18:12461–12475. https://doi.org/10.5194/acp-18-12461-2018

Wu L, Su H, Jiang JH (2013) Regional simulation of aerosol impacts on precipitation during the East Asian summer monsoon. J Geophys

Res Atmos 118(12):6454–6467. https://doi.org/10.1002/jgrd.50527

Xie SP (1996) Westward propagation of latitudinal asymmetry in a coupled ocean–atmosphere model. J Atmos Sci 53:3236–3250. https://doi.org/10.1175/1520-0469(1996)053%3c3236:WPO-LAI%3e2.0.CO;2

Xu H et al (2020) Juxtaposition of Western Pacific subtropical high on asian summer monsoon shapes subtropical East Asian precipitation. Geophys Res Lett 47(3):e2019GL084705. https://doi.org/10.1029/2019GL084705

Yoon J, Yeh SW (2010) Influence of the pacific decadal oscillation on the relationship between El Niño and the Northeast Asian summer monsoon. J Clim 23:4525–4537. https://doi.org/10.1175/2010JCLI3352.1

Zhang L, Zhou T (2015) Drought over East Asia: a review. J Clim 28(8):3375–3399. https://doi.org/10.1175/JCLI-D-14-00259.1

Zhang Y, Li T, Wang B (2004) Decadal change of the spring snow depth over the Tibetan Plateau: the associated circulation and influence on the East Asian summer monsoon. J Clim 17:2780–2793. https://doi.org/10.1175/1520-0442(2004)017%3c2780:DCOTSS%3e2.0.CO;2

Zheng B et al (2018) Trends in China's anthropogenic emissions since 2010 as the consequence of clean air actions. Atmos Chem Phys 18:14095–14111. https://doi.org/10.5194/acp-18-14095-2018

Zhou TJ, Gong DY, Li JP, Li B (2009) Detecting and understanding the multi-decadal variability of the East Asian Summer Monsoon-recent progress and state of affairs. Meteorol Z 18(4):455–467. https://doi.org/10.1127/0941-2948/2009/0396